Biophys Struct Mech (1983) 10: 143–168

Biophysics of Structure and Mechanism

© Springer-Verlag 1983

Ionic Conductance Through the Haemocyanin Channel in the Presence of the Trivalent Lanthanide Cation Terbium

G. Menestrina

Dipartimento di Fisica, Università degli Studi di Trento, I-38050 Povo (TN), Italy

Abstract. *Megathura crenulata* haemocyanin can be incorporated in phosphatidylcholine planar bilayers, forming ionic channels. Ca^{2+} and Tb^{3+} are known to bind to the protein and to compete for some common sites, here their effects on the electrical properties of the channel have been studied. Both cations have similar characteristics: they diffuse through the channel, linearize and shift its instantaneous current voltage curve and induce inactivation at negative voltages. Two-salt experiments are described in which small amounts of Ca^{2+} or Tb^{3+} are added to a KCl solution, allowing titration of these effects on the channel. S-shaped conductance voltage curves and strongly saturating conductance-concentration curves are explained on the basis of a two-state gating mechanism, coupled with the influence of a titratable fixed charge near the pore entrance. The model requires non-specific screening of the negative charge by counter-ions in solution and specific binding to it by divalent and small monovalent cations. Dissociation constants for the binding of Ca^{2+} and Tb^{3+} to the *M. crenulata* haemocyanin channel are calculated and found to be in good agreement with published data on binding of the same cations to other haemocyanins in physiological conditions.

Key words: Lipid bilayer – Haemocyanin channel – Terbium – Current saturation – Ion binding

Introduction

Haemocyanins are oxygen-carrying copper proteins with a high molecular weight that occur freely dissolved in the haemolymph of a number of invertebrates (for a recent review of these proteins see [38]). One of these, *Megathura crenulata* haemocyanin, is able to interact with planar lipid bilayers, forming voltage-dependent channels [1, 33]. Voltage dependence arises both from the transitions of the channel conductance between several discrete levels

and from the non-linearity of the fast current voltage curve of each level [21]. At the highest level the conductance of the channel depends not only on the applied voltage but is also strongly dependent on the type and concentration of cation and the pH of the solution [26, 27]. To explain the saturation properties of the haemocyanin channel with monovalent cations, Cecchi et al. [5] proposed a single-ion occupancy, three-barrier model for ion transport. On the other hand, on the basis of experiments with mono- and divalent cations Menestrina and Antolini [27] proposed a multi-ion occupancy model, where saturation originates from the effects of a negative fixed charge near the pore entrance. The latter model requires specific binding of divalent and small monovalent cations to the channel. Binding of divalent cations to haemocyanin is widely recognized [38] and NMR results have recently been presented [2] which demonstrate competition between Na^+ and Ca^{2+} for common sites on the protein.

A study of the properties of the haemocyanin channel in the presence of terbium ions is reported here. The aim of the work was twofold. first, lanthanide ions are excellent probes for Ca^{2+} effects on proteins [24]. Terbium itself has been widely used in recent years together with fluorescence techniques to study Ca^{2+} binding sites on several proteins such as elastase, parvalbumin and apoferritin [8, 29, 36] and on haemocyanin itself [19, 20]. Accordingly, one would expect terbium to affect channel properties in a way very similar to that of calcium and the other divalents [27], and this is indeed what was observed. Furthermore, two-salt experiments in which small amounts of $TbCl_3$ are added to a KCl solution indicate that titration of the effects of Tb^{3+} on the channel is possible and that dissociation constants obtained in this way can be directly compared to those found in the literature for other haemocyanins in free solution. Second, terbium is a trivalent cation and thus also provides the opportunity to study voltage and concentration dependence of the channel conductance with these multivalent cations. This seems to be a very critical test for a model of ion conduction through the pore. It is shown here that the multi-occupancy fixed-charge model can account for the experimental results. This is important, since it is currently agreed that specific and non-specific negative fixed charges are present near the pore entrance for natural ionic channels such as Na^+ [9] and K^+ [12, 13] nerve channels.

Materials and Methods

Black lipid membranes were painted on a 0.4 mm diameter circular hole in a Teflon septum separating two aqueous solutions using the usual technique [37]. The lipid used was egg phosphatidylcholine (PC), more than 99% pure, from P.L. Biochemicals, dissolved in n-decane to a concentration of 50 mg/ml. Electrolytic solutions were prepared using either KCl or $CaCl_2$ (Carlo Erba RPE) or $TbCl_3$ (Riedel de Haën) or mixtures of these salts. They were buffered at pH 7.0 with Bistris (Calbiochem) either at a concentration of 5% of that of the main electrolyte in the one-salt experiments, or at a fixed concentration of 10

mM in the two-salt experiments. Tb^{3+} is known to produce a 1 : 1 compound with EDTA [16]; for this reason conductimetric titrations, performed with a Philips PW 9509 digital conductivity meter were used to evaluate the Tb^{3+} concentration. Small amounts of EDTA (0.05−1 mM) were always present in the bathing solutions to eliminate traces of divalent cations, both Ca^{2+} and Tb^{3+} concentrations were in excess of that of the EDTA present. *M. crenulata* haemocyanin (A grade) in 50% glycerol was purchased from Calbiochem and stored at −20° C. Small amounts of a 4 mg/ml stock solution were added to one chamber only (*cis* side) at least 15 min after complete formation of the black film. The final protein concentration ranged from 2 to 50 μg/ml, depending on the electrolyte used [27]. Electrical access to the membrane was gained through Ag-AgCl electrodes. Current was amplified by a virtual grounded operational amplifier (AD 515 K) with a parallel circuit of 10^8 Ω, 20 pF or 10^7 Ω, 200 pF in the feed-back loop. The protein-containing compartment was taken as the reference for voltage sign. All the experiments were performed at room temperature (18°−22° C).

The procedures used to obtain single-channel conductance and instantaneous and steady-state current voltage curves of multi-channel membranes have been described in detail previously [27], together with the corrections that are usually necessary because of a slow increase in conductance caused by the formation of new channels. Briefly, single-channel conductance was measured by the height of the current steps observed at fixed voltage during the incorporation of the first 10−60 channels; the voltage was chosen in order to have channels in the higher conductance state. Instantaneous current voltage curves were obtained by applying short voltage pulses of 0.3−0.5 s duration and of different amplitudes, starting from a zero resting potential. Several (2−4) *I/V* curves were recorded during each experiment and then averaged. steady-state current voltage curves were obtained by applying long-lasting (usually some minutes) voltage pulses, which allowed for complete relaxation of the current to the steady-state value; the resting potential between one pulse and the next was chosen, depending on the cation present in the solution, with an aim to having all channels in the highest conductance state.

Two-salt experiments were performed, the solutions being mixed before preparation of the lipid membrane. Alternatively, one of the following procedures has been adopted:

1. *M. crenulata* haemocyanin was kept overnight in a buffer solution containing 5 mM $TbCl_3$. The protein was then added during the experiment to a Tb^{3+} free 0.1 M KCl solution with 0.05 mM EDTA. The final concentration of Tb^{3+} was 25 μM, i.e., less than that of EDTA.
2. Protein incorportion in the membrane was performed in a 0.1 M KCl solution containing symmetrical 0.5 mM $TbCl_3$. After incorporation of a large number of channels, EDTA was added to both compartments in excess of the Tb^{3+} present, i.e., 1.3−1.8 mM.
3. Protein incorporation in the bilayer was accomplished in a Tb^{3+}-free 0.1 M KCl solution. After extensive perfusion of the *cis* compartment, which was necessary to remove free protein from the solution, 2 mM $TbCl_3$ was added symmetrically to the bathing solution.

Results

Instantaneous Current Voltage Curves in One-Salt Solutions

M. crenulata haemocyanin-doped PC membranes show non-linear instantaneous current voltage curves [1]. It has already been shown [5, 27] that the shape of the I/V characteristic depends on both the concentration and the type of the electrolyte making up the bathing solution, but in general the positive branch of the curve is less steep than the negative branch.

Three instantaneous current voltage curves (obtained following the protocol described in Methods), with the chlorides of three different cations are presented in Fig. 1. Each curve has been scaled down to the current that would

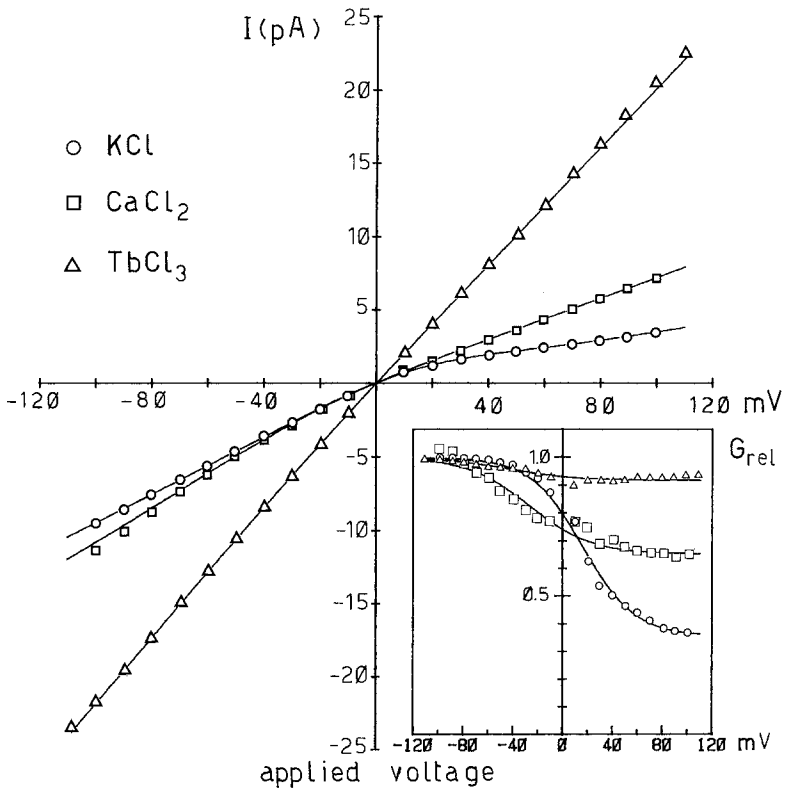

Fig. 1. Instantaneous current voltage curves of haemocyanin-treated bilayers in the presence of the chlorides of three different cations, K^+, Ca^{2+}, and Tb^{3+} at a concentration of 50 mM. Each curve has been scaled down to the current that would flow through a single channel and least squares fitted by a two-state model. Fit procedures give the maximum conductance of the channel which is 95, 110, and 220 pS respectively for K^+, Ca^{2+}, and Tb^{3+}. The relative conductance (Eq. 5) is calculated and plotted in the inset of the figure for the same experiments. *Solid lines,* as above, are the predictions of the two-state model with the least squares parameters. These, listed in the order K^+, Ca^{2+}, Tb^{3+}, are: *lower asymptote:* 0.359, 0.653, 0.918; *abscissa of the inflection point:* +16.1, −26.8, −43.9 mV; *slope at the inflection point:* 0.048, 0.040, 0.033 mV^{-1}

flow through a single channel, making use of the single-channel current measured at a fixed voltage by the height of the incorporation steps (see Methods). The three cations, all at a concentration of 50 mM, are K^+, Ca^{2+}, and Tb^{3+}. It is apparent that the non-linearity of the *I/V* curve is greatest with the monovalent cation, much less with Ca^{2+} and almost absent with Tb^{3+}. In the meantime the maximum slope of the curve, which occurs in the third quadrant and corresponds to the maximum conductance of the channel, increases in the order K^+, Ca^{2+}, Tb^{3+}.

A clearer presentation of the experimental data is achieved if one calculates the relative conductance, obtained by dividing the single-channel current by the voltage applied and by the maximum conductance. These data are plotted against potential in the inset of Fig. 1. For each salt the relative conductance has a sigmoid shape, which can be described by three parameters: the abscissa of the inflection point, the slope of the curve at this point and the value of the lower asymptote. Changing from the mono- to the di- and trivalent cation had the following effects: a dramatic increase in the lower asymptote (i.e., in the minimum relative conductance of the channel), which accounts for much of the corresponding linearization of the *I/V* curve; a strong shift of the inflection point towards negative voltages and only a slight decrease in the slope of the curve at the midpoint.

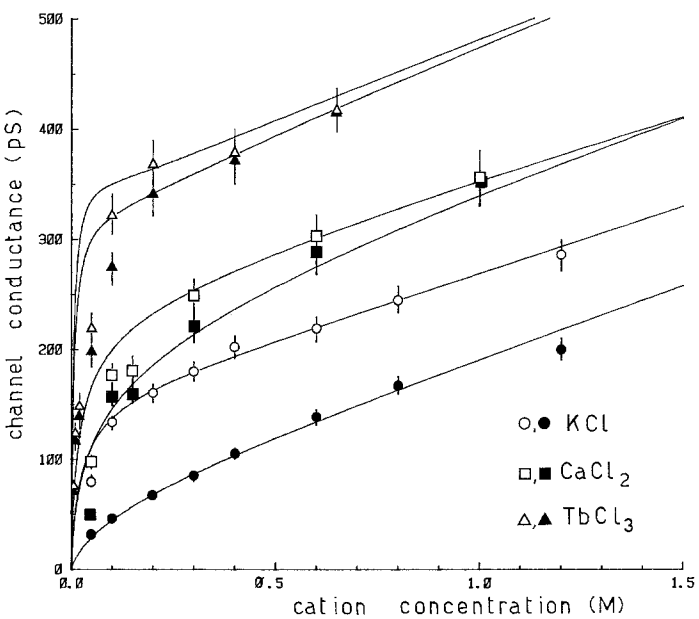

Fig. 2. Maximum and minimum conductance of the haemocyanin channel, open and solid symbols respectively, as a function of concentration for the three different cations K^+, Ca^{2+} and Tb^{3+}. *Solid lines* are drawn according to the "negative fixed charge model" described in the discussion (Eqs. 6–9). The parameters used to generate the lines on the figure are listed in Table 1. These parameters are chosen on the basis of a visual matching of computer generated theoretical lines to the experimental points as the best which can fit simultaneously the results of the one-salt experiment of this figure and two-salt experiments of Fig. 6

Plots of the relative conductance, like those in the inset of Fig. 1, allow one to calculate for each cation and each concentration two independent conductance values for the channel, corresponding to the high and low asymptote of the sigmoid. In Fig. 2, these two values, which should be the maximum and minimum conductance of the pore, G_{max} and G_{min} respectively, are plotted against salt concentration for the three cations in Fig. 1. All of these conductances show saturation, i.e., they increase sublinearly with the concentration. It is noteworthy, however, that they tend to increase linearly from a certain point. G_{max} at each concentration increases considerably, from K^+ to Ca^{2+}, to Tb^{3+}, which indicates a high permeability of the channel also to di- and trivalent cations. Furthermore, one can see that G_{min} approaches G_{max}, either by increasing the ionic strength, with a fixed cation, or, at a fixed concentration, going from K^+ to Ca^{2+} and even more to Tb^{3+}, which also increases the ionic strength. This implies that the *I/V* curves become linear when the ionic strength of the solution is increased. This is in good agreement with published data [5, 27].

Steady-State Current Voltage Curves in One-Salt Solutions

Current through *M. crenulata* haemocyanin-doped membranes is also a function of time. As previously shown [1, 28], application of long-lasting voltage pulses of appropriate value can produce a time-dependent decrease in the current flowing through the channels. This decrease, which takes place in seconds, is due to a voltage-dependent closing of the channel through several discrete levels of decreasing conductance. When K^+ is the only cation in solution, positive voltages tend to close the channel and negative ones leave it open, whereas the reverse is true if a divalent cation salt makes up the electrolytic bath [27].

The results of this kind of study in the presence of the trivalent cation Tb^{3+} are shown in Figs. 3 and 4. Long-lasting voltage pulses (usually about 2 min) were applied to a multi-channel membrane and current was continuously recorded until the steady-state was reached (Fig. 3a). Between one pulse and the next, the membrane was kept at zero voltage for a resting period of several seconds. In complete agreement with the observations with divalent cations, positive pulses gave rise to constant currents, whereas negative pulses produced a time-dependent decrease in current. Digitization of the transients (one

---

Fig. 4. Voltage dependence of the haemocyanin-induced steady-state conductance. The ratio of the steady state to the instantaneous conductance in a 5 mM $TbCl_3$ solution is shown (*full triangles* and *left-hand scale*). The solid S-shaped curve is a least squares fit to the points with a two-state model (Eqs. 2 and 3). The parameters obtained are $G^*_{ss} = 0.435$, $V_0 = 0$ mV, $q_{ss} = -2.3$ e.u. The two time constants of the current relaxations, measured as in Fig. 3, are also plotted (*full* and *open circles, Central scale*). *Dashed lines* are drawn by eye. The results of two experiments have been averaged. In the inset the relative steady-state conductance in a solution of 50 mM KCl is given for comparison. *Solid line* is a least squares fit, the values of the parameters are $G^*_{ss} = 0.510$, $V_0 = 58$ mV, $q_{ss} = 1.6$ e.u. G^*_{ss}, V_0, and q_{ss} are defined in the discussion

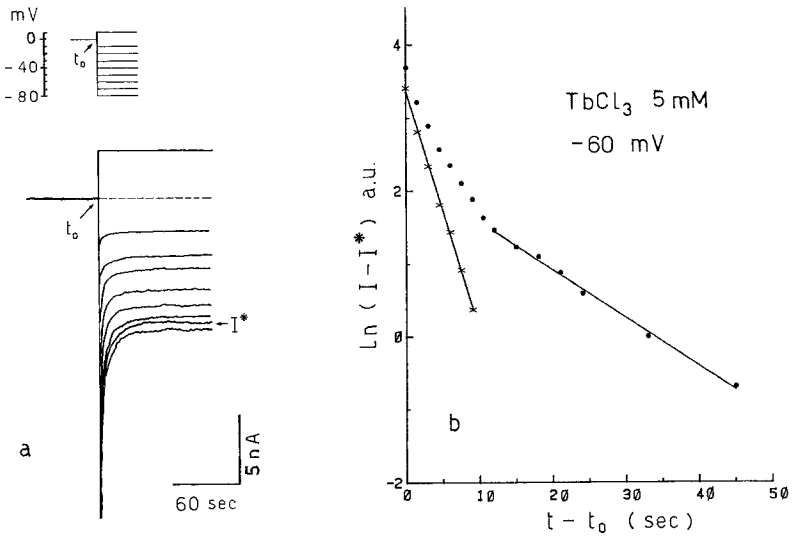

Fig. 3a and b. Current relaxations after application of long-lasting voltage pulses to an haemocyanin-doped membrane, bathed by a 5 mM $TbCl_3$ solution. **a** Current traces after step changes from zero to different potentials are super-imposed. The pulse protocol is given at the top. Current at positive potentials remains constant while at negative potentials relaxes to a lower steady-state value. **b** *Circles:* half-logarithmic plot of the relaxation amplitude $I - I^*$, where I^* is the steady-state current, measured in arbitrary units at −60 mV applied voltage. A first-order relaxation may be extrapolated only from a certain point. *Crosses:* fast relaxation after subtraction of the slow relaxation. The least squares fit values of the two time constants, fast and slow, are 3.0 and 15.2 s respectively

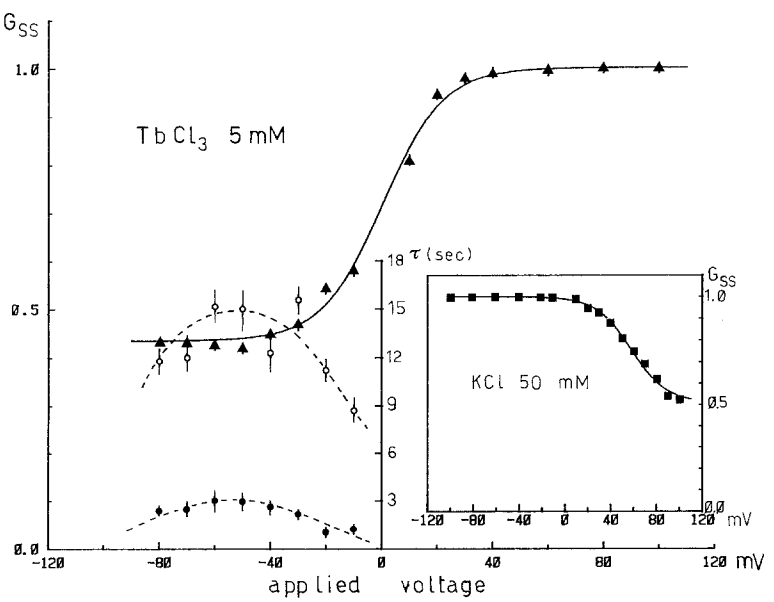

example is shown in Fig. 3b) showed that also in this case the process cannot be described by a single time constant. Usually two exponentials are necessary and sufficient to fit the current decay, the faster being calculated after subtraction of the slower one. The steady-state relative conductance, i.e., the ratio between steady-state and instantaneous current values, and the two time constants for the relaxations are all voltage-dependent. A plot of these variables against applied potential (Fig. 4) shows that the conductance voltage curve is S-shaped, while the two time constants both go through a maximum. As with mono- and divalent cations, an increase in the Tb^{3+} concentration is accompanied by a decrease in the non-linearity of the steady-state *I/V* curve. At a concentration of 0.1 M

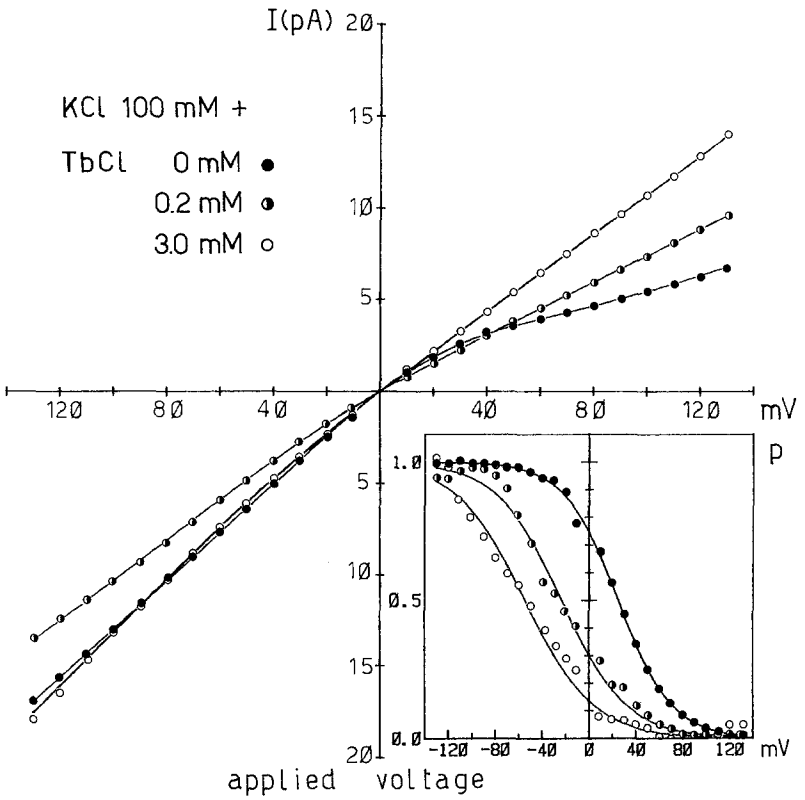

Fig. 5. Instantaneous current voltage curves of haemocyanin-treated bilayers in the presence of mixed solutions of KCl and $TbCl_3$. $TbCl_3$ was added symmetrically before membrane formation at the concentrations indicated, curves are scaled down to the current that would flow through a single channel. The effect of adding Tb^{3+} to the solution is to linearize the *I/V* curve. Conductance voltage curves are S-shaped and allow extrapolation of two values of channel conductance, i.e., G_{max} and G_{min} for the high and low asymptote respectively. For the three curves corresponding to 0, 0.2, 3.0 mM Tb^{3+}, values of G_{max} are 131, 106, and 137 pS respectively whereas those of G_{min} are 51, 73 and 107 pS. The parameter *p*, defined by Eq. (1), is plotted in the inset of Fig. 5 for the same experiments, using the same symbols. This parameter contains all of the voltage dependence of the *G/V* curve. *Solid lines* are least squares fits to the points using Eq. (3) which give the following values of the fit parameters: $V_0 = 24, -23.5, -54.4$ mV and $Q = 0.044, 0.036, 0.034$ mV^{-1} for $TbCl_3$ 0, 0.2, and 3.0 mM, respectively

$TbCl_3$, the *I/V* curve is practically linear and transitions can no longer be seen (data not shown). As already mentioned, the voltage dependence of the steady-state conductance with $TbCl_3$ is opposite to that observed with KCl, which is shown in the inset of Fig. 4 for comparison.

Instantaneous Current Voltage Curves in Two-Salt Solutions

Since the properties of the channel vary so greatly depending on whether mono-, di- or trivalent cations make up the solution, one may wonder what happens when these salts are mixed. The effects of adding small amounts of $TbCl_3$ symmetrically to a 0.1 M KCl bathing solution on the instantaneous *I/V* curve of haemocyanin channels are shown in Fig. 5. The addition of Tb^{3+} induces a strong linearization of the *I/V* characteristic, which, however, is always less steep in the first quadrant than in the third. Even under these conditions, conductance voltage curves are S-shaped, allowing calculations of two asymptotic conductance values. These values, normalized with the aid of the single-channel conductance measured during haemocyanin incorporation, represent G_{max} and

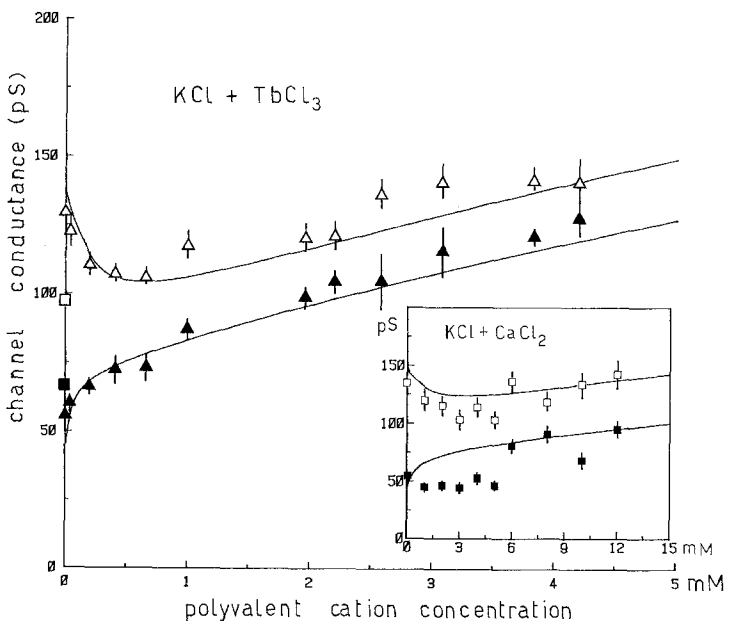

Fig. 6. Maximum and minimum conductance of the haemocyanin channel (*open* and *solid symbols*) in two-salt experiments. Different concentrations of $TbCl_3$ are added to a 0.1 M KCl solution prior to membrane formation. *Solid lines* are the predictions of the negative fixed charge model (Eqs. 10–13) with the parameters listed in Table 1. Specific binding of Tb^{3+} is assumed; a good fit of the curves to the points is achieved with a dissociation constant K_{Tb} between 0.03 and 0.05 mM. Squares refer to experiments run with procedure A given in methods (mean of 3 membranes). In the inset the same kind of data are relevant, but obtained by adding $CaCl_2$ instead of $TbCl_3$ to a 0.1 M KCl solution. *Solid lines* as above; reasonably good fit is achieved with K_{Ca} 0.2–0.5 mM. Dissociation constants used are listed in Table 2

G_{min} under the given conditions, and are plotted in Fig. 6 against the final concentration of $TbCl_3$.

It is apparent that G_{max} goes through a minimum when one increases the concentration of Tb^{3+} added to the KCl solution. A similar behaviour was observed with the Gramicidin A channel when increasing amounts of the highly permeant thallous ion were added to a 1 M NaCl solution [31]. This result is a strong indication that a simple mutual exclusion mechanism among ions does not apply to the action of Tb^{3+}. On the other hand G_{min} increases monotonically, approaching G_{max} and producing in this way the observed linearization of the *I/V* curve. Similar results were also achieved when Ca^{2+} cations were added to a 0.1 M KCl solution; these data are presented in the inset of Fig. 6.

In all these experiments, Tb^{3+} or Ca^{2+} were mixed with the solution before protein was added. Since both these cations are known to bind specifically to haemocyanin in solution [19], one can argue that these effects may be due to an irreversible binding of the cations to the protein prior to channel formation. Control experiments were conducted, interacting protein samples which have been equilibrated overnight in a Tb^{3+} rich buffer with planar lipid bilayers bathed in a Tb^{3+}-free KCl solution (procedure A in Methods). Indeed, low values of G_{max} and high values of G_{min}, i.e., linearized *I/V* curves, have also been obtained in this way despite the lack of Tb^{3+} from the bathing solution (Fig. 6).

Using the two asymptotic values G_{max} and G_{min} a parameter p can be calculated, given by:

$$p(V) = \frac{G(V) - G_{min}}{G_{max} - G_{min}}, \tag{1}$$

Fig. 7a–c. Effects of Tb^{3+} added symmetrically to 0.1 M KCl on the voltage dependence of the conductance of the haemocyanin channel. **a** Half-logarithmic plot of the ratio $p/(1-p)$, where p is defined by Eq. (1) against Tb^{3+} concentration. *Solid lines* are least squares fit to the points using Eq. (15), with $K_A = 0.709$ mM and $K_B = 0.045$ mM, both constant. The values of K_1 obtained by the fit are plotted in the inset against applied voltage (*open circles*). *Dotted lines* are also least squares fit of Eq. (15) but with $K_A = 0.709$ mM constant only. The values of K_1 and K_B obtained are plotted in the inset as above, solid circles and squares respectively. Left-hand scale of the inset refers to K_1 values, whereas right-hand scale is for K_B values. *Solid* and *dotted lines* are the regression lines through the points. The parameters obtained are: $K_1(0) = 1.56$, $z_1 = 0.90$ (*solid line*); $K_1(0) = 1.25$, $z_1 = 1.10$ and $K_B(0) = 0.08$ mM, $z_B = -0.30$ (*dotted lines*). **b** Observed shift of the inflection point of the *G/V* curve, ΔV_0 in the text, against Tb^{3+} concentration (*full circles*). The *solid line* is a least squares fit to the points using Eq. (20) with $z_1 = 0.95$ which gives $K_A = 0.709$ mM and $K_B = 0.045$ mM. The *dotted line* is the prediction of Eq. (21) using $K_A = 0.709$ mM, $K_B(0) = 0.08$ mM $z_1 = 1.10$ and $z_B = -0.30$. The point represented by an *open square* is the result of procedure *A* (mean of 3 experiments), whereas the *diamonds* represent experiments run with procedure *B* (mean of 3 experiments). *Open* and *solid diamonds* are the shift before and after addition of EDTA respectively. Finally, the *triangles* are the results obtained with procedure *C*, *open* and *full symbols* corresponding to the shift before and after adding Tb^{3+}. In the inset, ΔV_0 induced by symmetrical addition of $Ca\,Cl_2$ to a 0.1 M KCl solution is shown. The *solid line* is a least squares fit to the points by Eq. (20),using the mean value of $z_1 = 1.2$, which gives $K_A > 500$ mM and $K_B = 0.34$ mM. **c** Slope of the *G/V* curve at the inflection point against Tb^{3+} concentration (*solid circles*). The *solid line* is the mean value of the experimental points, $z_1 = 0.95$, whereas the *dotted line* is the prediction of Eq. (17) using $z_1 = 1.10$, $z_B = -0.30$ and $V = -30$ mV. *Squares*, *diamonds*, and *triangles* represent the same experiments as above and have the same significance

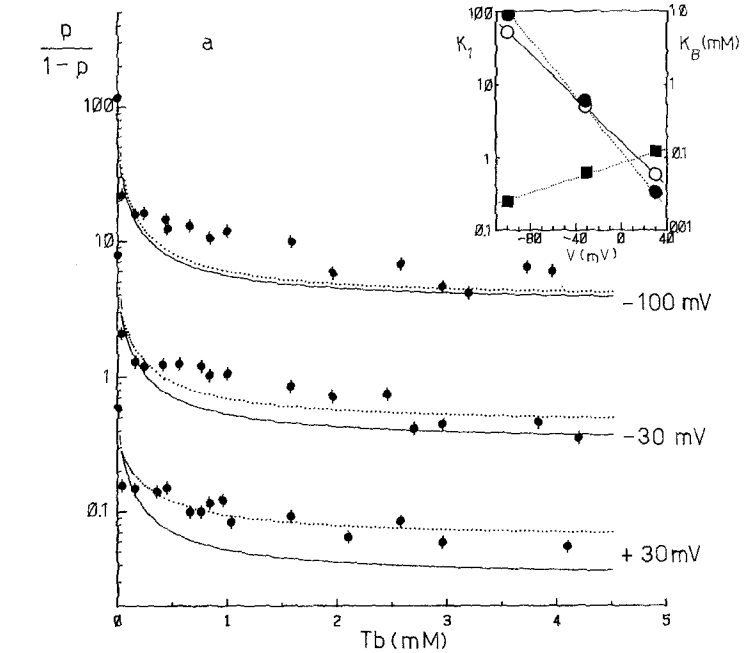
p / 1 − p
a
100
10
1
0.1
−100 mV
−30 mV
+30mV
Tb (mM)
K_1
K_B (mM)
V (mV)

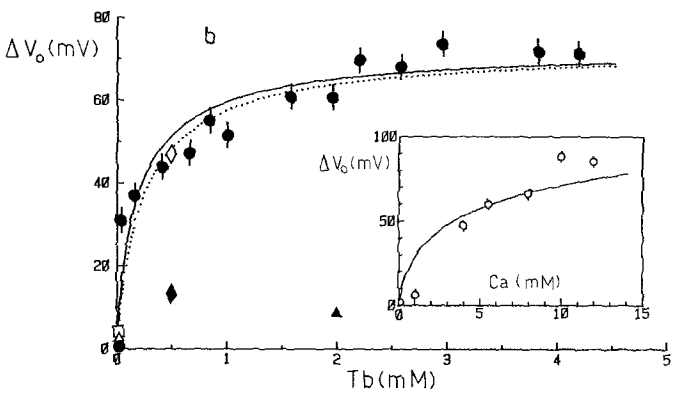
ΔV_0 (mV)
b
Tb (mM)
Ca (mM)

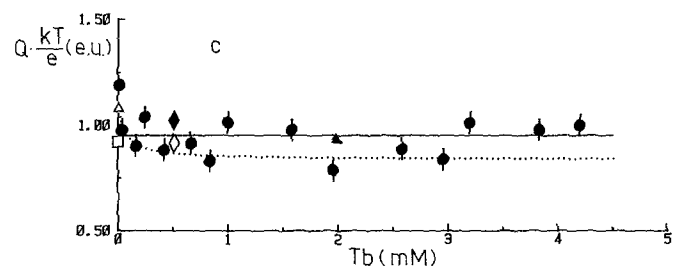
$Q \cdot \frac{kT}{e}$ (e.u.)
c
Tb (mM)

where $G(V)$ is the voltage-dependent conductance of the channel. The significance of p in a two-state model of the channel is given in the Discussion. P contains all of the voltage dependence of G and, as shown in the inset of Fig. 5, varies sigmoidally between one and zero. A rapid inspection of Fig. 5 indicates that addition of Tb^{3+} to the KCl solution causes the abscissa of the inflection point of p to shift strongly towards negative voltages and the slope of the curve to become less steep at this point. This result could be foreseen on the basis of the one-salt experiments run with either, KCl or $TbCl_3$ presented in Fig. 1. Indeed, addition of Tb^{3+} to a KCl solution seems to change these parameters from the values they have with K^+ alone to the values they have with Tb^{3+} alone. The effects of Tb^{3+} on p are summarized in Fig. 7. In Fig. 7a, the ratio $p/(1-p)$, which is relevant for the discussion, is presented in a half-logarithmic plot against Tb^{3+} concentration for three different applied voltages. In Fig. 7b, the observed shift of the inflection point abscissa along the voltage axis is plotted as a function of Tb^{3+} concentration. In the inset, the same kind of data are reported for the case when Ca^{2+} is added to a 0.1 M KCl solution instead of Tb^{3+}. Finally, in Fig. 7c the slope of the curve at the inflection point, expressed in terms of electronic units, is presented against Tb^{3+} concentration again.

Control experiments were conducted with procedure A. The pre-treatment failed to give any appreciable shift of the p curve, as shown in Fig. 7b. On the other hand, addition of excess EDTA to a bathing solution containing 0.5 mM $TbCl_3$ (procedure B) showed an almost complete reversibility of the Tb^{3+}-induced shift of p (Fig. 7b). It is also interesting to note how the ratio G_{min}/G_{max} varied in these control experiments. This parameter, the lower asymptote in Fig. 1 (inset) gives a measure of the non-linearity of the I/V curve. Its value, which is 0.52 in 0.1 M KCl alone (strong non-linearity) and 0.74 in 0.1 M KCl plus 0.5 mM $TbCl_3$ (weak non-linearity) is only slightly reduced (to 0.68) by addition of excess EDTA (procedure B). The last value is remarkably similar to that obtained with the protein pre-treated in$TbCl_3$ (procedure A), which is 0.67. Such results indicate that of the two major effects observed, one, the linearization, depends on the irreversible binding of Tb^{3+} to the protein that takes place before channel formation, while the other, the shift along the voltage axis, depends on the presence of Tb^{3+} in the solution bathing the channel.

As a last control, experiments were conducted in which Tb^{3+} was added after haemocyanin incorporation had taken place in a Tb^{3+}-free KCl solution (procedure C). Under these conditions, the non-linearity of the I/V curve remained strong, $G_{min}/G_{max} = 0.5$ in Tb^{3+} 2 mM, and there was only a minor shift of Vo (about 10 mV) towards negative voltages.

Steady-State Current Voltage Curves in Two-Salt Solutions

Together with the effects on the instantaneous I/V curve, the addition of Tb^{3+} to a KCl solution also leads to strong modifications of the steady-state properties of the channel. In the presence of 0.1 M KCl alone, negative voltage pulses of long duration produce constant currents, while positive pulses lead to a time-dependent decrease in current [28]. This situation is completely reversed if small

amounts of Tb^{3+} are added to the K^+ bathing solution. One example is shown in Fig. 8. Just as in the case of Tb Cl_3 alone, in these mixed solutions negative voltage also produce a decrease in current which is directly dependent on the size of the negative potential applied (Fig. 8a). Furthermore, as in this case, the transient can be fitted by the sum of two exponentials of different time constants (Fig. 8b). Steady-state conductance, normalized by dividing by the instantaneous conductance, at different concentrations of Tb^{3+} added to the KCl solution is plotted in Fig. 9. It is apparent that the more Tb^{3+} is added the more the non-linearity of the conductance voltage curve develops. The value of the lower asymptote (G^*_{ss}) can be used as a measure of the non-linearity of the curve; a smaller value indicating a greater non-linearity. This parameter is plotted against Tb^{3+} concentration in the inset of Fig. 9 to give a titration curve for the effects of $TbCl_3$ on the steady-state properties of the channel.

Control experiments were also conducted in this case, using procedures A and B. With both of these procedures the absence of Tb^{3+} from the bathing solution led to no change in current at negative voltages (inset of Fig. 9). Removing Tb^{3+} with EDTA produced a change in G^*_{ss} from 0.60 ± 0.02 to 0.90 ± 0.04, which represents an almost complete reversibility of the effects of Tb^{3+} on the negative branch of the steady-state conductance voltage curve. It is worth noting that both procedures completely inhibited the non-linearity at positive voltage typical of KCl solutions.

Discussion

Instantaneous current voltage curves of *M. crenulata* haemocyanin are non-linear and their shape depends strongly on the type and concentration of the cations present in the bathing solution. Two models have recently been presented which can explain this complex behaviour. The first, proposed by Cecchi et al. [5] following experiments with K^+ and Li^+ sulphates, is a three-barrier two-site model, based on absolute reaction rate theory, with the further assumption that only one ion can occupy the channel at a given time. The second, proposed by Menestrina and Antolini [27] in order to explain the results of experiments performed with the chlorides of four monovalent cations (Li^+, Na^+, K^+, Cs^+) and four divalent cations (Mg^{2+}, Ca^{2+}, Sr^{2+}, Ba^{2+}), assumes that the channel bears a titratable negative fixed charge at its mouth and that it posesses two conformations in an electric field. No restriction is imposed on the diffusion of ions into the pore.

The latter model originated from the observation made by Menestrina and Antolini [26] that the conductance of the open channel is pH dependent, a fact that has been now confirmed by two other groups [6, 14]. As shown recently by Lindemann [23] positive titration curves, like those observed with haemocyanin channels, indicate the presence of fixed charges near the pore mouth which control the local ionic concentration (*c*-control). Furthermore, Lindemann demonstrated that in a one-ion multi-barrier multi-site channel model, *c*-control is the sign of low occupancy. Since the strong saturation of conductance concentration curves [5, 27] suggests high occupancy for the haemocyanin

channel, developing a multi-ion model for this channel would still be of interest. For this reason a refinement of the model presented in [27] is discussed which can explain published data in addition to the trivalent cation effects and the two-salt experiments reported in this paper.

The Fixed Charge Model for One-Salt Solutions

Conductance voltage curves of the haemocyanin channel at a fixed electrolyte composition are S-shaped (Fig. 1). This suggests the use of a simple two-state gating model, of the type discussed for example in [11], to calculate the conductance, G, of the channel:

$$G(V,\alpha) = G_B(\alpha) + [G_A(\alpha) - G_B(\alpha)] \cdot p(V,\alpha) . \tag{2}$$

$$p(V,\alpha) = 1/(1 + \exp\{q(\alpha) \cdot [V - V_0(\alpha)]/kT\}) , \tag{3}$$

where G_A and G_B are the channel conductance in states A and B; q is the apparent gating charge; V is the applied potential; qV_0 is the conformational energy change between the two states; p represents the probability of occupancy of state A. The index α has been added to account for the differences observed with different cations. It is assumed that the gating charge q, the voltage sensor which promotes the transition between states A and B, experiences all of the applied potential. The slope of the G/V curve at the inflection point is given as the quantity $Q = q/kT$, the real slope being directly proportional to it:

$$\left.\frac{dG}{dV}\right|_{V = V_0} = Q \cdot (G_B - G_A)/4 .$$

The current through the channel is then simply given by:

$$I(V,\alpha) = G(V,\alpha) \cdot V . \tag{4}$$

Many channel I/V curves, like those shown in Fig. 1, are first best fitted with Eq. (4), with the aid of Eqs. (2) and (3), and then normalized by dividing by V and by the maximum extrapolated conductance to give a relative conductance G_{rel}:

$$G_{rel}(V,\alpha) = G(V,\alpha)/G_{max}(\alpha) , \tag{5}$$

as plotted in the inset of Fig. 1. The true single-channel conductance is then obtained by multiplying G_{rel} by the factor which gives the single-channel conductance measured at one fixed voltage during the initial incorporation of haemocyanin. An inspection of the inset of Fig. 1 reveals that consistency is attained if one assumes that q is a positive charge, $G(A) = G_{max}$ and $G(B) = G_{min}$. In this way Eqs. (1) and (2) coincide.

Calculated values of G_A and G_B at different concentrations of the chlorides of K^+, Ca^{2+}, and Tb^{3+} are plotted in Fig. 2. Each one shows a sublinear increase

with concentration, consistent with published data on mono- and divalent cations. Figure 2 shows that Ca^{2+} and also Tb^{3+} diffuse easily through the pore. This is noteworthy since the haemocyanin channel has recently been compared [6, 22] to the K^+-channel of the sarcoplasmic reticulum characterized by Miller and co-workers [7, 30]. This is a one-cation multi-barrier multi-site channel which, however, excludes completely divalent cations [7]. Also Gramicidin A, an example of a single-file multi-barrier but also multi-ion channel, is completely impermeable to divalent cations [4]. Thus, the lack of selectivity of the haemocyanin channel within mono, di- and trivalent cations argues against single-filing and single-ion occupancy in this pore.

An explanation for the observed saturation properties, alternative to single-ion occupancy, is to consider the channel as a cylindrical pore filled with water, with a fixed charge at its mouths determining a local concentration of ions different from that in the bulk, i.e., *c*-control. Saturation then comes from the screening of the fixed charge by counter-ions. We can write in this case:

$$G_\beta(\alpha) = \frac{\pi r^2}{l}\,\omega(\alpha)\cdot z(\alpha)\cdot e\cdot c\,. \tag{6}$$

$$\omega(\alpha) = \gamma\cdot\omega_0(\alpha)\,. \tag{7}$$

$$c = c_0\cdot\exp[-z(\alpha)\cdot e\psi_\beta(\alpha)/kT]\,, \tag{8}$$

where β may be A or B; r and l are the radius and length of the pore; z is the valence of the ion; e is the elementary charge; ω_0 and ω are the conventional mobilities of the ion in the solution and in the pore; c_0 and c are the concentrations of the ion in the bulk solution and at the pore entrance; ψ_β is the potential created by the fixed charges at the mouth of the pore, and the other symbols have been defined previously. From Eq. (8) one can see that if ψ_β is great enough only counter-ions contribute substantially to the pore conductance. In order to explain the cation selectivity of the channel (3), we have to assume that it bears negative fixed charge.

To calculate ψ_β one should first notice that discrete charge theories are much more appropriate then smeared charge theories when applied to macromolecules such as intramembrane channels [10, 32]. On the other hand, it has been shown [27] that symmetric distributions of fixed charges around a point, the pore entrance for example, calculated as in [32] give practically the same potential as a single point charge at the same average distance. In the light of these findings, the more simplistic form for the potential is chosen, i.e., the potential in the proximity of the surface of a macro-ion calculated from the Debye-Hückel theory [35]:

$$\psi_\beta(\alpha) = \frac{Z_\beta(\alpha)e}{4\pi\varepsilon}\,\frac{\exp\varkappa[a - r_\beta(\alpha)]}{(1+\varkappa a)\cdot r_\beta(\alpha)}\,, \tag{9}$$

where Z_β is the total fixed charge on the macromolecule, i, e.g.; $\varkappa$ is the Debye-Hückel coefficient; ε is the dielectric constant of water; a is the closest

possible distance between ions in the solution and the macro-ion; r_β is the distance from the macro-ion at which the potential is calculated, i.e., the average distance between the fixed charges and the pore entrance.

This calculation for the potential at the pore's mouth is obviously oversimplified. Nevertheless, one should notice that despite the severe approximations used to derive it, the Debye-Hückel expression of Eq. (9) has proved to give essentially the same predictions as recently developed precise electrolyte theories, even at high concentrations, at least for a 1 : 1 salt [34]. Furthermore, I feel that a search for a better expression for the potential is unnecessary for the point to be made here, i.e., that *c*-control can be used to predict the saturation of the haemocyanin channel conductance with concentration.

Equations (6), (7), (8), and (9) can be used together to fit the experimental data of Fig. 2. Three parameters are allowed to vary: $\pi r^2/l\ \gamma\ (\alpha)$, $Z_\beta\ (\alpha)$, and $r_\beta\ (\alpha)$; a is given the constant value 0.38 nm and $z\ (\alpha)$, $\omega_0\ (\alpha)$, c_0 are given appropriate values (conventional mobilities of ions in solution can be found in the literature). The parameters used to generate the solid lines of Fig. 2 are listed in Table 1. These parameters have also been chosen to fit the experimental points of Fig. 6. An inspection of Table 1 indicates that all three free parameters decrease in the order K^+, Ca^{2+}, Tb^{3+}. This means that (1) the mobility of the cation in the pore relative to that in the bulk solution decreases from mono- to di- and even more to trivalent cations; (2) the fixed charge on the pore decreases in the same way; (3) the distribution of the point charges changes with the cation such that the average distance from the pore entrance decreases in the same order. On the other hand the transition from state *A* to state *B* for each cation produces only a decrease in the fixed charge Z_β.

These findings are in good agreement with previously reported data [27] on mono- and divalent cations, although the expression of the potential used here differs from that in [27]. Of particular interest is the dependence of the total amount of fixed charge on the cation present in solution. It follows the order (using also data from [27]):

$$Cs^+ \simeq K^+ > Na^+ > Li^+ > Mg^{2+} \simeq Ca^{2+} \simeq Sr^{2+} \simeq Ba^{2+} > Tb^{3+}.$$

Table 1. Parameters used in Eqs. (6)–(9), and (10)–(13) to generate the solid lines in Figs. 2 and 6 respectively

Parameter	Units	Channel state	Cation		
			K^+	Ca^{2+}	Tb^{3+}
$\frac{\pi r^2}{l}\gamma$	pm	*A*	7.0	2.8	1.6
		B	6.8	2.8	1.7
Z		*A*	4.64	1.70	1.34
		B	2.40	1.41	1.29
r	nm	*A*	0.73	0.43	0.39
		B	0.73	0.41	0.39

It has been suggested that a specific binding of divalent and small monovalent positive ions to negatively charged sites on the protein is responsible for the observed decrease in the charge on the channel. It is worth noting that binding of Na^+, Ca^{2+}, and Tb^{3+} has now been directly measured on haemocyanins in solution by several authors and with different techniques. The results of these studies are summarized in Table 2. Two-salt experiments in which small amounts of Tb^{3+} or Ca^{2+} are added to a K^+ bathing solution, presented in this paper, are designed to titrate the effects of these cations on the haemocyanin channel.

Application of the Fixed Charge Model to Two-Salt Experiments

Addition of millimolar Tb^{3+} to a 0.1-M KCl solution, in which haemocyanin interacts with a bilayer, strongly reduces the non-linearity of the *I/V* curve (Fig. 5). Nevertheless the conductance remains S-shaped allowing the use of Eqs. (2) and (3) to fit the data. This procedure gives the two quantities G_A and G_B which are the maximum (G_{max}) and the minimum (G_{min}) conductances of the channel respectively. Extrapolation to high negative voltages in order to calculate G_{max} under different conditions is particularly important since the voltage dependence of the conductance, curve *p*, is shifted towards negative voltages when increasing amounts of Tb^{3+} are added to the solution (inset of Fig. 5). This fact introduces a systematic error if one compares conductances at a fixed voltage, as was done for example by Cecchi et al. [5] when studying the effects of Li^+ in similar experiments.

As shown in Fig. 6, G_{max} goes through a minimum when the concentration of Tb^{3+} or Ca^{2+} added to the bathing solution is increased. A strikingly similar behaviour has been observed when studying the effects of the thallous ion on the conductance of the Gramicidin A channel, in the presence of Na^+ [31]. Tl^+ is itself a highly permeant ion, hence the observed initial decrease of the conductance has been attributed in that case to a specific binding of the cation onto the channel. This is probably also the case here. Assuming that the two cations permeate independently through the channel, but that the fixed charges and their distribution are altered by a specific binding of Tb^{3+} or Ca^{2+}, one can calculate the conductance of the channel as follows:

$$G_\beta = \sum_\alpha \frac{\pi r^2}{l}\, \omega(\alpha) z(\alpha) e c_0(\alpha) \exp[-z(\alpha) e \psi^*_\beta / kT] \,. \tag{10}$$

$$\psi^*_\beta = \frac{Z^*_\beta}{4\pi\varepsilon} \frac{\exp \varkappa(a - r^*_\beta)}{(1 + \varkappa a) r^*_\beta} \,. \tag{11}$$

$$Z^*_\beta = Z_\beta(b) + [Z_\beta(K^+) - Z_\beta(b)]/[1 + c_0(b)/K_b] \,. \tag{12}$$

$$r^*_\beta = r_\beta(b) + [r_\beta(K^+) - r_\beta(b)]/[1 + c_0(b)/K_b] \,, \tag{13}$$

Table 2. Dissociation constants for various cations which bind to haemocyanin, measured by several authors with different techniques. The values in the last three rows have been obtained by fitting experimental data in Figs. 6, 7, and 9 of this work, respectively

Technique	Organism	Dissociation constant (mM)				Binding sites per subunit[a]	Reference
		Na^+	Mg^{2+}	Ca^{2+}	Tb^{3+}		
Gel filtration	*Levantina hierosolima G*[b]			13		20	17
Fluorescence	*Panulirus interruptus A*[c]			11	0.1–0.3		19
Fluorescence[d]	*Panulirus interruptus A*			16.7	0.2		20
^{23}Na NMR	*Panulirus interruptus A*	10	0.08–0.12	0.025–0.050		1	2
^{43}Ca NMR[d]			0.2 –1.0	0.2 –1.0		10 ± 7	
Channel conductance	*Megathura crenulata G*			0.35	0.040		
G/V curve shift				0.34; > 500[e]	0.045; 0.709[e]		f
G_{ss}/V curve non-linearity					0.037		

[a] On the basis of electron microscopic studies (25) a rough estimate can be made that seven to nine subunits compose the haemocyanin channel
[b] *G* refers to gastropod while *A* refers to arthropod
[c] Similar effects have been observed with haemocyanin from the gastropod *Helix pomatia*
[d] Experiments indicate the ocurrence of binding sites in clusters
[e] The two values are for states *B* and *A* respectively
[f] This paper

where summation over α denotes the sum of the contributions of K^+ and of the binding cation (Tb^{3+} or Ca^{2+}) named b; ψ_β^* is the potential at the pore entrance determined assuming that the fixed charge Z_β^* and its average distance from the channel mouth r_β^* both vary from the value with K^+ alone to the value with the binding cation alone, following a simple titration curve, eqs. (12) and (13), with a dissociation constant K_b. Other symbols as above.

Equations (10), (11), (12), and (13) with the parameters listed in Table 1 and the dissociation constants listed in Table 2 are used to generate the solid lines of Fig. 6, which are in good agreement with experimental data.

Since binding can occur in solution and thus prior to channel formation one can try to see if pre-treatment of the protein with Tb^{3+} modifies channel properties in a Tb^{3+}-free K^+ solution. Indeed, using procedure A, one can observe such an effect (Fig. 6). The measured conductances lie very near the extrapolations to zero concentration of Tb^{3+} of the linear part of the solid lines in the figure. That is, they correspond to the conductances the channel would have if K^+ alone is present insolution but Z_β^* and r_β^* are reduced by bound Tb^{3+} to the values they have with Tb^{3+} alone.

Transition between states A and B is thought to be a voltage-dependent change in the conformation of the channel. Table 1 shows that this change has the apparent effect of decreasing the fixed charge near the pore mouth.

It is possible to say that in configuration B much of the negative charge is too far from the pore entrance to influence the local ion concentration. Since the charge is presumably composed of a large number of titratable negative sites, binding of CA^{2+} or Tb^{3+} to these sites not only decreases the total amount of fixed charge, but substantially reduces the difference in charge between the two configurations A and B, determining in this way the strong linearization of the I/V curve shown in Fig. 1.

On the other hand, one may expect binding of cations to the channel to affect the equilibrium between the two configurations. This happens if one of the two conformational states has a larger affinity for the bound ion than the other. Hanke and Miller [15] have shown recently that if this is the case, changing the concentration of the binding ion shifts the voltage dependence of the channel conductance along the voltage axis. Two-salt experiments reported here, in which Tb^{3+} or Ca^{2+} modify the strongly non-linear G/V curve typical of K^+, are suitable to look for such effects. The inset of Fig. 5 clearly indicates that the G/V curve of haemocyanin-doped membranes is shifted along the voltage axis by Tb^{3+}.

Following Hanke and Miller [15] one can try to explain this result introducing a four-state model for the channel:

$$\begin{array}{ccc} & \overset{K_1}{} & \\ B & \rightleftarrows & A \\ {\scriptstyle K_B}\uparrow\downarrow & & \uparrow\downarrow{\scriptstyle K_A} \\ B_b & \rightleftarrows & A_b \\ & \underset{K_2}{} & \end{array} \qquad (14)$$

where B and B_b refer to the unbound and bound states of configuration B, and A and A_b refer similarly to the configuration A. It is supposed that there is no difference in conductance between the A states or the B states. Binding equilibria are described by the two dissociation constants K_A and K_B, and conformational transitions by the two equilibrium constants K_1 and K_2.

As shown in [15], where p is the probability of being in one of the electrically indistinguishable states A, one has:

$$\frac{p(V)}{1-p(V)} = K_1 \frac{(1+[b]/K_A)}{(1+[b]/K_B)}, \tag{15}$$

where $[b]$ is the concentration of the binding cation.

In general, the equilibrium constants are thought to be voltage-dependent according to:

$$K_i(V) = K_i(0) \exp(-z_i e V/kT), \tag{16}$$

where i is $1, 2, A$ or B and z_i represents the valence of the gating charge of the relation.

The slope at the inflection point of the G/V curve is easily calculated [15]:

$$Q(V) = \frac{e}{kT}\left(z_i - \frac{z_A}{1+K_A(V)/[b]} + \frac{z_B}{1+K_B(V)/[b]}\right). \tag{17}$$

To a first approximation one can assume that both binding reactions are voltage independent, i.e., $z_A = z_B = 0$, hence Q is a constant:

$$Q = \frac{e}{kT} z_1 . \tag{18}$$

In this simple case the abscissa of the inflection point is given by Eq. (15):

$$V_0 = \frac{1}{Q} \ln\left[K_1(0) \frac{(1+[b]/K_A)}{(1+[b]/K_B)}\right]. \tag{19}$$

Using Eqs. (18) and (19), the voltage shift induced by the binding cation b, and defined as $\Delta V_0 = V_0([b]=0) - V_0([b] \neq 0)$, is then:

$$\Delta V_0 = \frac{1}{z_1}\frac{kT}{e} \ln \frac{1+[b]/K_B}{1+[b]/K_A}. \tag{20}$$

The slope of the G/V curve at different concentrations of Tb^{3+} is shown in Fig. 7c. Its mean value (solid line) is $Q = 0.038\ mV^{-1}$, which corresponds at 20° C to $z_1 = 0.95$. ΔV_0 values are plotted in Fig. 7b; using Eq. (20) with the mean value of Q found, one can obtain K_A and K_B by a least squares fit to the points (solid line). This procedure gives $K_A = 0.709$ mM and $K_B = 0.038$ mM. Finally, the quantity $p/(1-p)$ is plotted in Fig. 7a for three different applied

voltages. Using Eq. (15) with the above found values for K_A and K_B, the equilibrium constant $K_1(V)$ at three different voltages can be derived again by a least squares adaptation to the points (solid lines in Fig. 7a). Values of K_1 calculated in this way are plotted in the inset of the same figure on a half-logarithmic scale against applied voltage. They show that indeed K_1 varies exponentially with voltage as demanded by Eq. (16). The regression line (solid line) yields $z_1 = 0.90$ in good agreement with the measured mean value, which indicates that autoconsistency of the model is achieved.

Now, in a second step, one can try to see whether fitting to the points can be improved by releasing one of the assumptions made above, i.e., $z_B = 0$. Then, assuming that only $z_A = 0$, one can repeat the least squares fit to the points in Fig. 7a again using $K_A = 0.709$ mM but leaving both $K_1(V)$ and $K_B(V)$ free to vary. This has been done (dotted lines), and the fit has indeed improved. The two equlibrium constants derived in this way are plotted in the inset of Fig. 7a. Both vary exponentially with voltage but have opposite sign. Regression lines (dotted lines) give $z_1 = 1.10$, $z_B = -0.30$ and $K_B(0) = 0.08$ mM. An approximate expression for the voltage shift ΔV_0 can also be given for this second case:

$$\Delta V_0 \simeq \frac{1}{z_1 + z_B} \frac{kT}{e} \ln \frac{1 + [b]/K_B(0)}{1 + [b]/K_A}, \tag{21}$$

where the condition $[b]/K_B(0) \gg 1$, which is almost always fulfilled in these experiments, has been used. The dotted line in Fig. 7b is the prediction of Eq. (21) with the values of z_1, z_B, $K_B(0)$, and K_A given above. Finally, Eq. (17) with a constant value of $V = -30$ mV, which corresponds to the mean observed V_0, can be used to approximate the apparent gating charge of the transition at different Tb^{3+} concentrations (dotted line in Fig. 7c).

The overall fit of experimental points in Fig. 7 seems to be better in the second hypothesis. In any case one should notice that K_A is voltage-independent and also that the voltage dependence of K_B is verly low: the value of z_B found indicates that Tb^{3+} experiences about one-tenth the applied voltage during the reaction. This implies that binding of cations to the channel takes place on or near its surface, as postulated. The model further demands that bound and unbound states are in equilibrium and hence that binding of cation b to the channel is reversible. Figure 7b, c shows that this is the case. In fact, not only is procedure A ineffective in producing a voltage shift in a Tb^{3+}-free solution, but also procedure *B* shows that EDTA in excess removes about 90% of Tb^{3+} effects on the *p* curve.

The existence of two kinds of binding sites is suggested by the experiments discussed previously. One, responsible for the *G/V* curve linearization, is accessible only before channel formation; the other, responsible for the shift and the decreased slope of the *p* curve,is always accessible. However, addition of Tb^{3+} after channel formation (procedure *C*) besides failing to linearize the *G/V* curve, as expected, produces only a slight shift of the *p* curve (Fig. 7b). This indicates that occupation of sites of the first kind facilitates occupancy of sites of the second kind, which can be understood only if co-operativity exists between the two species. This hypothesis is not unrealistic since co-operativity between

binding sites has been observed on haemocyanin in physiological conditions [20].

Steady-State Current Voltage Curves

Application of long-lasting voltage pulses can produce strong decrease in the current through *M. crenulata* haemocyanin channels. It has been shown [28], in the case of a 0.1 M KCl solution, that transitions between different conformations of the channel, which are seen as fluctuations among several discrete conductance states in single-channel experiments, are responsible for the multi-exponential relaxations observed in multi-channel experiments. When K^+ cations make up the electrolyte, positive voltages decrease the conductance of the channel (inset of Fig. 4); on the other hand, when divalent cations are present, negative voltages reduce channel conductance, whereas positive ones leave it unaffected [27].

Figure 3 shows that this is also the case in a $TbCl_3$ solution. Application of negative potentials produces large voltage- and time-dependent inactivation of the haemocyanin-induced conductance (Fig. 3a). Each current transient can be fitted by the sum of two exponential decays with different time constants, both in the range of seconds. Either the final conductance or the two time constants are voltage-dependent, as shown in Fig. 4. The relative steady state conductance, G_{ss}, calculated as a fraction of the instantaneous conductance depends sigmoidally on the applied voltage. A reasonably good fit to the points is obtained using the simple two-state expression of Eqs. (2) and (3), although also with $TbCl_3$ probably more than two configurations are involved in the observed transitions. Experiments with different concentrations of $TbCl_3$ (data not shown) indicate that an increase of the ionic strength produces a decrease of the non linearity of the G_{ss}/V curve. The slope of the G_{ss}/V curve at the inflection point is relatively constant, corresponding to a gating $q_{ss} = -1.9 \pm 0.2$ e.u. (mean $\pm$ SD of seven experiments at different Tb^{3+} concentrations). A two-state model predicts that current relaxation in voltage clamp experiments is a single exponential whose time constant is a bell-shaped function of applied voltage [11]. As shown in Figs. 3 and 4, two time constants are measured with haemocyanin channels, which implies that at least three pore states are involved; in any case both time constants are bell-shaped functions of the applied voltage.

The behaviour observed with Tb^{3+} is similar to that with Ca^{2+} and the other divalents. It has been suggested [27] that it is again due to a specific binding of these cations to the channel. Hence two-salt experiments can also be used in this case to titrate the effects of Tb^{3+}. Figures 8 and 9 show that addition of millimolar $TbCl_3$ to a 0.1 M KCl solution changes the G_{ss}/V curve from a positive slope as with K^+ alone to a negative slope as with Tb^{3+} alone. Current relaxations at negative voltages with 5 mM $TbCl_3$ added to the KCl solution are the sum of two exponentials like those obtained with 5 mM $TbCl_3$ alone, and also the two time constants are aimilar in both cases (Figs. 8 and 3). G_{ss}/V curves are S-shaped and, as shown in Fig. 9, their non-linearity increases with Tb^{3+}

concentration. All the curves are fitted by the two-state model (Eqs. 2 and 3) and the gating charge observed is $q_{ss} = -1.7 \pm 0.2$ e.u. (mean ± SD of 27 experiments at different Tb^{3+} concentrations), very similar to the value measured with Tb^{3+} alone.

The lower asymptote of the G_{ss}/V curve, G^*_{ss}, is used in the inset of Fig. 9 as a measure of the effects induced by Tb^{3+}. Assuming that the non-linearity of the G_{ss}/V curve in the negative voltage region is due to a specific binding of Tb^{3+} to the channel, one can write:

$$G^*_{ss} = G_0 + (1 - G_0)/(1 + [Tb^{3+}]/K_d)\,, \tag{22}$$

where G_0 is the asymptotical value of G^*_{ss}, reached when all sites are titrated, $[Tb^{3+}]$ is the bulk concentration of Tb^{3+} and K_d is the dissociation constant of this binding process. The solid line in the inset of Fig. 9 is generated by a least squares fit to the points with Eq. (21), which gives $G_0 = 0.526$ and $K_d = 0.037$ mM.

These effects seem to be for a large part reversible. In fact procedure *A* gives only a small non-linearity at negative potentials, and procedure *B* removes to a large extent the effects of Tb^{3+} (inset of Fig. 9). Nevertheless, with both procedures the non-linearity in the positive region typical of K^+ was almost completely inhibited (data not shown). Once again this indicates the existence of two kinds of binding sites, responsible for different effects on the channel.

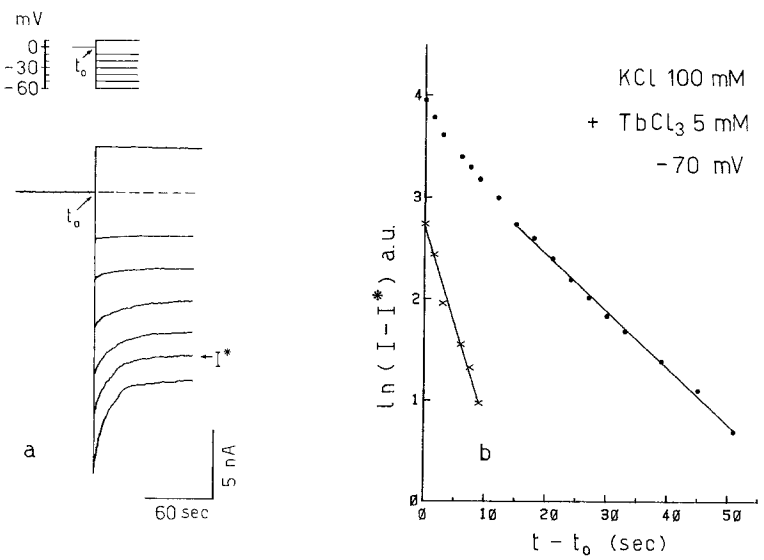

Fig. 8a and b. Current relaxations in a two-salt solution made up of 0.1 M KCl plus 5 mM $TbCl_3$. **a** Superimposed current traces obtained with the pulse protocol shown at the top. **b** *Solid circles:* digitization of one current transient at −70 mV and plotted in half-logarithmic scale against time. The *solid line* is the regression line through the points of the interval, time constant 17.5 s. *Crosses:* half-logarithmic plot of the fast component of the relaxation after subtraction of the slow, time constant 4.7 s. Current scale as in Fig. 3

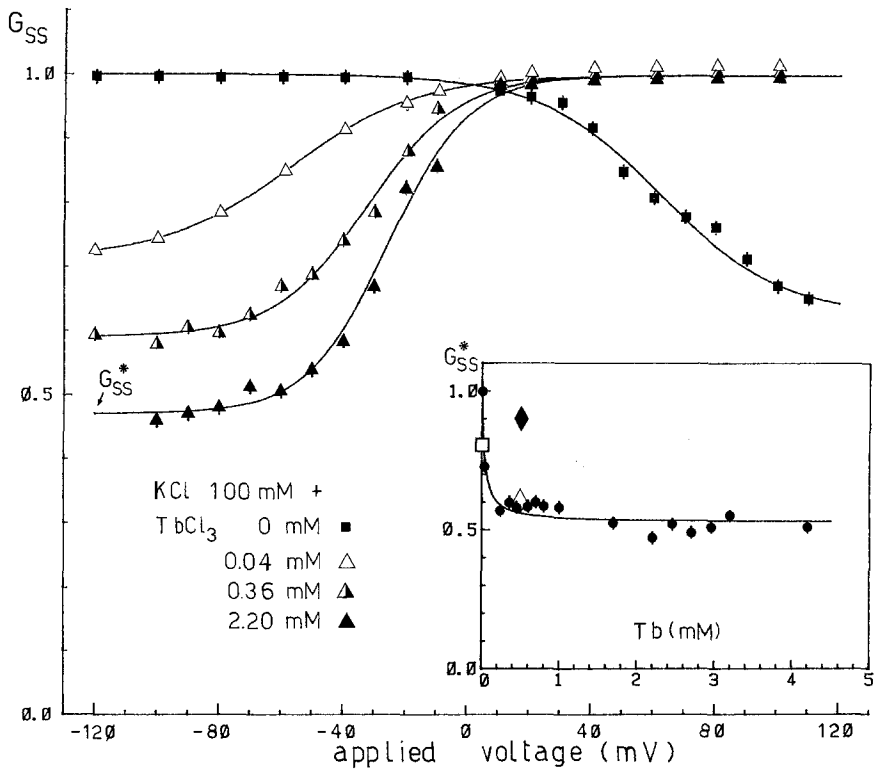

Fig. 9. Steady-state relative conductance of the haemocyanin channel in a two-salt solution. Different concentrations of Tb^{3+} are symmetrically added to a 0.1 M KCl solution. Increasing the concentration of the lanthanide increases the non-linearity of the G_{ss}/V curve at negative potentials. Solid lines are best fit to the points using Eqs. (2) and (3). The lower asymptote, G^*_{ss}, is plotted in the inset of the figure against Tb^{3+} concentration, *solid curcles*. The *solid line* is the least squares adaptation of Eq. (22) which gives $G_0 = 0.526$ and $K_d = 0.037$ mM. *Squares* and *diamonds* have the same significance as in Fig. 7b and c

Conclusions

It is shown here that in the presence of a trivalent cation such as terbium the properties of the haemocyanin channel can be accounted for by a simple model which calls for the presence of a fixed titratable negative charge at the pore entrance. Both non-specific screening and specific binding by cations of the bathing solution contribute to determine channel conductance. This fixed charge could be made up of a relatively large number of negative sites, with variable distribution and occupancy. Binding of cations to some of these sites is almost irreversible after channel formation, possibly because they become inaccessible in the lipid moiety, whereas binding to the others is largely reversible.

Dissociation constants for the specific binding of Tb^{3+} and Ca^{2+} to the pore, measured in this work by their effects on channel conductance, are reported in Table 2 and compared to published data for these and two other cations on different haemocyanins. There is substantially good agreement between the two

sets of data, both qualitatively (the affinity sequence $Tb^{3+} > Ca^{2+} > Na^{+}$ seems to hold true for haemocyanin in solution as well as for the channel [27] and quantitatively.

It has been proposed [17] that divalent cations chelate a carboxylate ion and an imidazolium ion from an histidine and that H^{+} competes for this same site. In addition, fluorescence and NMR studies indicate that Na^{+}, Ca^{2+} and Tb^{3+} also compete for common sites [2, 19] on haemocyanin, and that some of these are clustered [2]. The observed affinity sequence for binding to the channel is indeed consistent with the involvement of a carboxylic group in the binding reaction [18]. Furthermore, it has been shown [14] that the treatment of *M. crenulata* haemocyanin with diethylpyrocarbonate, which specifically modifies histidine residues, strongly affects the electrical properties of the channel. In the light of these findings, I suggests that negative sites formed by carboxylic groups and histidines are very important for determining haemocyanin channel properties.

Acknowledgements. I wish to thank Mrs. E. Agostini for her excellent work in typing this manuscript. This work was supported in part by Consiglio Nazionale delle Ricerche and Ministero di Pubblica Istruzione Italiani.

References

1. Alvarez O, Diaz E, Latorre R (1975) Voltage-dependent conductance induced by hemocyanin in black lipid films. Biochim Biophys Acta 389: 444–448
2. Andersson T, Chiancone E, Forsen S (1982) Characterization of cation binding sites on Panulirus interruptus hemocyanin by ^{43}Ca and ^{23}Na NMR. Eur J Biochem 125: 103–108
3. Antolini R, Menestrina G (1979) Ion conductivity of the open Keyhole limpet hemocyanin channel. FEBS Lett 100: 377–381
4. Bamberg E, Läuger P (1977) Blocking of the gramicidin channel by divalent cations. J Membrane Biol 35: 351–375
5. Cecchi X, Alvarez O, Latorre R (1981) A three-barrier model for the hemocyanin channel. J Gen Physiol 78: 657–681
6. Cecchi X, Bull R, Franzoy R, Coronado R, Alvarez O (1982) Probing the pore size of the hemocyanin channel. Biochim Biophys Acta 693: 173–176
7. Coronado R, Rosenberg RL, Miller C (1980) Ionic selectivity, saturation and block in a K^{+}-selective channel from sarcoplasmic reticulum. J Gen Physiol 76: 425–446
8. de Jersey J, Martin RB (1980) Lanthanide probes in biological systems: the calcium binding site of pancreatic elastase as studied by terbium luminescence. Biochemistry 19: 1127–1132
9. Drouin H, Neumcke B (1974) Specific and unspecific charges at the sodium channels of the nerve membrane. Pflügers Arch 351: 207–229
10. Enos BE, McQuarrie DA (1981) The effect of discrete charges on the electrical properties of membranes. II. J Theor Biol 93: 499–522
11. Ehrenstein G, Lecar H (1977) Electrically gated ionic channels in lipid bilayers. Q Rev Biophys 10: 1–34
12. Fohlmeister JF, Adelman WJ Jr (1982) Periaxonal surface calcium binding and distribution of charge on the faces of squid axon potassium channel molecules. J Membr Biol 70: 115–123
13. Gilbert DL, Ehrenstein G (1969) Effect of divalent cations on potassium conductance of squid axon: determination of surface charge. Biophys J 9: 447–463
14. Griffin MCA, Sattelle DB (1983) Effects of pH and diethylpyrocarbonate on the conductance states of planar lipid bilayers containing hemocyanin. Biochim Biophys Acta 727: 56–62

15. Hanke W, Miller C (1983) Single chloride channels from torpedo electroplax: activation by protons. J Gen Physiol 82: 25–45
16. Hauser H, Hinkley CC, Krebs J, Levine BA, Phillips MC, Williams RJP (1977) The interaction of ions with phosphatidylcholine bilayers. Biochim Biophys Acta 468: 364–377
17. Klarman A, Shaklai N, Daniel E (1972) The binding of calcium ions to hemocyanin from Levantina hierosolima at physiological pH. Biochim Biophys Acta 257: 150–157
18. Kostyuk PG (1981) Calcium channels in the neuronal membrane. Biochim Biophys Acta 650: 128–150
19. Kuiper HA, Finazzi-Agro A, Antonini E, Brunori M (1979) The replacement of calcium by terbium as an allosteric effector of haemocyanins. FEBS Lett 99: 317–320
20. Kuiper HA, Zolla L, Finazzi-Agro A, Brunori M (1981) Interaction of lanthanide ions with Panulirus interruptus hemocyanin: evidence for vicinity of some of the binding sites. J Mol Biol 149: 805–812
21. Latorre R, Alvarez O, Ehrenstein G, Espinoza M, Reyes J (1975) The nature of the voltage dependent conductance of the hemocyanin channel. J Membr Biol 25: 163–182
22. Latorre R, Miller C (1983) Conduction and selectivity in potassium channels. J Membr Biol 71: 11–30
23. Lindemann B (1982) Dependence of ion flow through channels on the density of fixed charges at the channel opening. Biophys J 39: 15–22
24. Martin RB, Richardson FS (1979) Lanthanides as probes for calcium in biological systems. Q Rev Biophys 12: 181–209
25. McIntosh TJ, Robertson JD, Ting-Beall HP, Walter A, Zampighi G (1980) On the structure of the hemocyanin channel in lipid bilayers. Biochim Biophys Acta 601: 289–301
26. Menestrina G, Antolini R (1981) Ion transport through hemocyanin channels in oxidized cholesterol artificial bilayer membranes. Biochim Biophys Acta 643: 616–625
27. Menestrina G, Antolini R (1982) The dependence of the conductance of the hemocyanin channel on applied potential and ionic concentration with mono and divalent cations. Biochim Biophys Acta 688: 673–684
28. Menestrina G, Maniacco D, Antolini R (1983) A kinetic study of the opening and closing properties of the hemocyanin channel in artificial lipid bilayer membranes. J Membr Biol 71: 173–182
29. Miake-Lye RC, Doniach S, Hodgson KO (1983) Anomalous X-ray scattering from terbium-labeled parvalbumin in solution. Biophys J 41: 287–292
30. Miller C (1978) Voltage-gated cation conductance channel from fragmented sarcoplasmic reticulum: steady-state electrical properties. J Membr Biol 40: 1–23
31. Neher E (1975) Ion specificity of the gramicidin channel and the thallous ion. Biochim Biophys Acta 401: 540–544
32. Nelson AP, McQuarrie DA (1975) The effect of discrete charges on the electrical properties of a membrane. I. J Theor Biol 55: 13–27
33. Pant HC, Conran P (1972) Keyhole limpet hemocyanin (KLH) lipid bilayer membrane (BLM) interaction. J Membr Biol 8: 357–362
34. Pitzer KS (1977) Electrolyte theory-improvements since Debye and Hückel. Acc Chem Res 10: 371–377
35. Richards EG (1980) Introduction to the physical properties of large molecules in solution. Cambridge University Press, New York
36. Stefanini S, Chiancone E, Antonini E, Finazzi-Agro A (1983) Binding of terbium to apoferritin: a fluorescence study. Arch Biochem Biophys 222: 430–434
37. Szabo G, Eisenman G, Ciani S (1969) The effects of the macrotetralide actin antibiotics on the electrical properties of phospholipid bilayer membranes. J Membr Biol 1: 346–352
38. van Holde KE, Miller KI (1982) Hemocyanins. Q Rev Biophys 15: 1–129

Accepted 1 August 1983